PNAS RESEARCH ARTICLE | NEUROSCIENCE

Anterior cingulate cortex orexin signaling mediates early-life stress-induced social impairment in females

Fei Luo[a,b,1], Jun-yang Deng[b], Xuan Sun[a], Jian Zhen[a], and Xiao-dan Luo[b]

Edited by Hirofumi Morishita, Icahn School of Medicine at Mount Sinai, New York, NY; received December 2, 2022; accepted March 30, 2023 by Editorial Board Member Jeremy Nathans

Early-life stress has long-term impacts on the structure and function of the anterior cingulate cortex (ACC), and raises the risk of adult neuropsychiatric disorders including social dysfunction. The underlying neural mechanisms, however, are still uncertain. Here, we show that, in female mice, maternal separation (MS) during the first three postnatal weeks results in social impairment accompanied with hypoactivity in pyramidal neurons (PNs) of the ACC. Activation of ACC PNs ameliorates MS-induced social impairment. Neuropeptide Hcrt, which encodes hypocretin (orexin), is the top down-regulated gene in the ACC of MS females. Activating ACC orexin terminals enhances the activity of ACC PNs and rescues the diminished sociability observed in MS females via an orexin receptor 2 (OxR2)-dependent mechanism. Our results suggest orexin signaling in the ACC is critical in mediating early-life stress-induced social impairment in females.

pyramidal neuron | orexin | anterior cingulate cortex | sociability | mice

Stress hormones have extensive and complicated impacts throughout the lifetime (1, 2). In particular, brain development is sensitive to stressors in the neonatal and early infancy period (3, 4). Many studies have indicated that stressful events experienced during early-life enhance the risk of severe deficits in social functions such as social interaction and social rank (5, 6).

Cingulate cortex, an important part of the limbic system, is composed of many structurally and functionally distinct subregions. It is noteworthy that the anatomical definition of rat and mouse cingulate cortex subregions differs from that in other mammals, including humans (7). The anterior cingulate cortex (ACC, formally referred to as Cg1 and Cg2) is implicated in fundamental cognitive function, including decision-making, motivation, and cost–benefit calculation (8, 9). Brodmann area 24 is the major subregion of the ACC (10), and is believed to be important in processing social information from both human and animal model studies (11–13). Especially, a recent study from Guo et al. has demonstrated that ACC pyramidal neurons (PNs) hypoactivity contributes to the social interaction impairment in Shank3 mutant mice (12).

Here, we focused on mouse ACC (area 24), which is similar in cytoarchitecture and connectivity to the human area 24 implicated in social behaviors (11, 14), and sought to reveal neurobiological mechanisms underlying early-life stress-induced social impairment via adapting an unpredictable maternal separation (MS), a widely used early-life stress paradigm (1, 15). Our study indicates that orexin signaling in the ACC mediates the diminished sociability in MS females, and highlights the importance of the ACC as a potential therapeutic target for developing interventions for social impairment induced by early-life stress in females.

Result

MS-Induced Social Impairment Is Associated With Blunted Activation of ACC PNs in Females. We first performed the social approach (SA) assay to examine the impacts of MS on social interaction with social stimulus in females. Mice were either facility-reared (SFR) or subjected to unpredictable MS (Fig. 1*A*). In the SA assay, MS females spent less time engaging with the social stimulus than SFR females, indicating a reduced sociability phenotype (Fig. 1*B*). No significant changes were detected in the locomotor activity (*SI Appendix*, Fig. S1*A*), anxiety-like behavior (*SI Appendix*, Fig. S1 *B*–*G*), and food intake (*SI Appendix*, Fig. S2) between SFR and MS mice. We next evaluated sex differences in MS-induced changes in social behavior. We found that MS males also decreased social interaction time, but the magnitude of diminished sociability was significantly lower than that in females (*SI Appendix*, Fig. S3), suggesting MS females are more vulnerable to developing social impairment compared to MS males.

Significance

Early-life stress is known to cause long-lasting social deficits. In this study, we employed a well-known rodent model of early-life stress based on mother separation during the first 3 wk of postnatal life, to investigate how early-life stress caused the diminished sociability in female mice. This study documents that pyramidal neuron-specific engagement of orexin signaling in the anterior cingulate cortex is important for modulating early-life stress-induced social impairment in females.

Author affiliations: [a]Center for Neuropsychiatric Diseases, Institute of Life Science, Nanchang University, Nanchang 330031, China; and [b]Department of Psychiatry, Yichun First municipal People's Hospital, YiChun 336000, China

Author contributions: F.L. designed research; F.L., J.-y.D., X.S., J.Z., and X.-d.L. performed research; X.S., J.Z., and X.-d.L. analyzed data; and F.L. wrote the paper.

The authors declare no competing interest.

This article is a PNAS Direct Submission. H.M. is a guest editor invited by the Editorial Board.

[1]To whom correspondence may be addressed. Email: luofei@ncu.edu.cn.

This article contains supporting information online at https://www.pnas.org/lookup/suppl/doi:10.1073/pnas.2220353120/-/DCSupplemental.

Published May 8, 2023.

To determine whether decreased sociability in MS mice is connected with neuronal activity alterations in the ACC, a key area involved in social activities (12), we carried out in vivo calcium imaging in freely behaving mice (Fig. 1*C*). To do this, an adeno-associated virus encoding the calcium indicator GCaMP6f under the calmodulin kinase II promoter (AAV1-CaMKII-GCaMP6f) was injected into the ACC area (Fig. 1*D* and *SI Appendix*, Fig. S4). The resulting GCaMP6f expression was specific to PNs (Fig. 1*D*). To collect baseline calcium activity, mice were acclimated in the SA testing apparatus (including an empty cup) for 30 min, and the last 5-min GCaMP6f fluorescence in the ACC was recorded. As shown in Fig. 1*E*, MS female mice had a lower baseline calcium signal than SFR controls (Fig. 1*E*). The averaged baseline calcium activity revealed that MS females had considerably

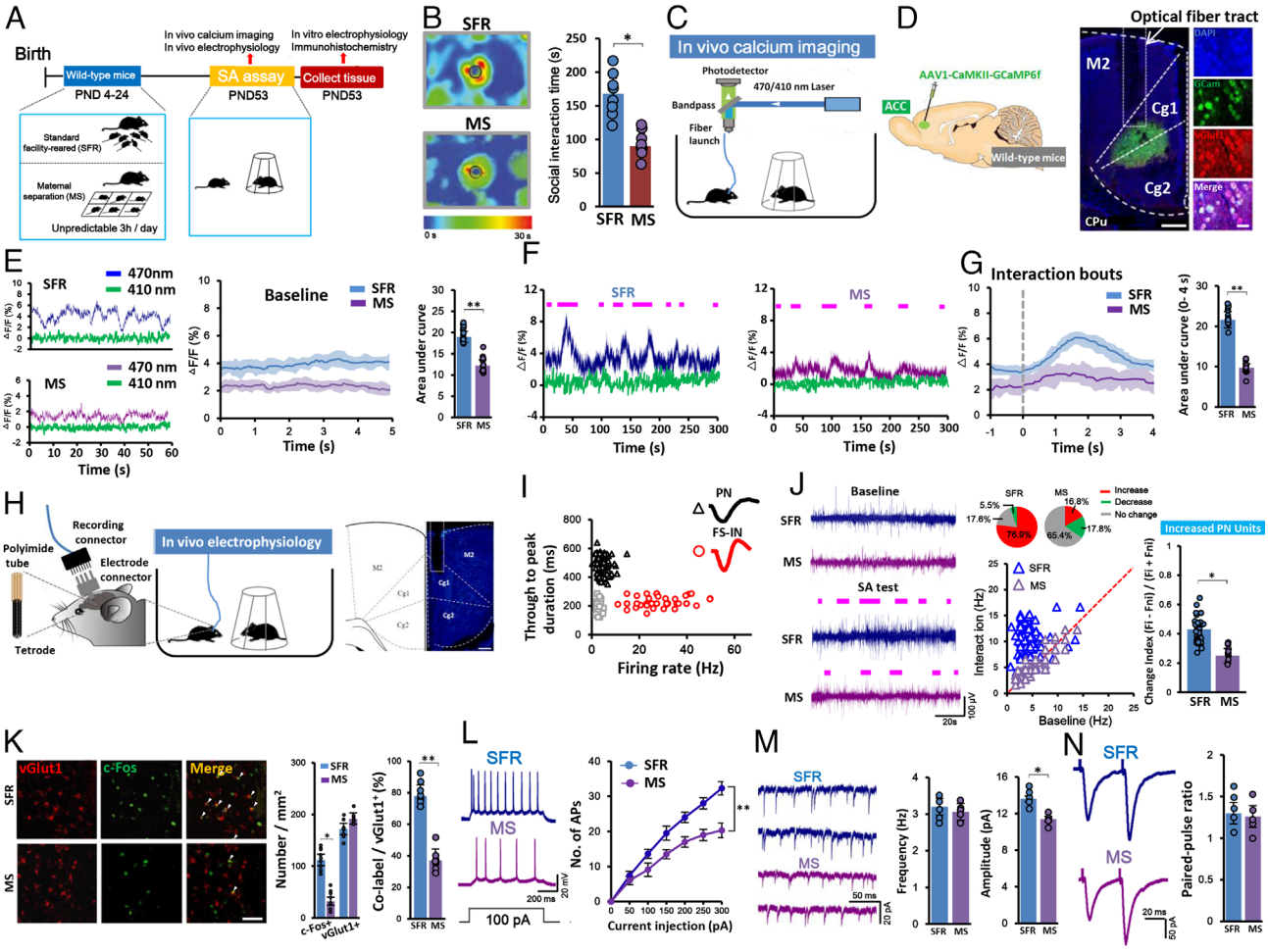

Fig. 1. MS induces social impairment accompanied by the blunted activation of ACC PNs in females. (*A*) Schematic of the experimental procedure. MS was carried out from postnatal day (PND) 4 to 24 d, followed by group housing, and the subsequent social approach (SA) test at PND 53. In vivo calcium imaging or in vivo electrophysiology was performed during the SA test, and in vitro electrophysiology or immunohistochemistry was performed 30 min after the SA test. (*B*) Bar graphs depicting the time spent interacting with social stimuli during the SA test in SFR and MS females (n = 8 females/group. Two-tailed unpaired *t* test). *Insets*: heatmaps showing time spent in different locations of the apparatus during SA tests. The circles mark the locations of social stimulus. (*C*) Diagram of calcium imaging in a freely behaving mouse. (*D*) Surgical manipulations (*Left*) and placement of an optic fiber for fiber photometry in the ACC of a mouse injected with AAV1-CaMKII-GCaMP6f (*Right*). Confocal images showing that GCaMP6f (GCaM)-labeled neurons colocalized with PNs (vGlut1$^+$ neurons). Cg1: cingulate cortex, area 1; Cg2: cingulate cortex, area 2; M2: secondary motor cortex; CPu: caudate putamen. (Scale bars: 200 or 50 μm). (*E*, *Left*) Baseline recording photometry traces from typical SFR and MS female mice expressing GCaMP6f in the ACC. The fluorescence change from the median of the total time series is represented by the △F/F. *Middle*: perievent plots of averaged calcium signals during baseline recording in SFR and MS females (n = 16 to 17 bouts/4 females/group). *Right*: bar graphs depicting the calcium signal in the ACC during baseline recordings of SFR and MS female mice (Mann–Whitney U-test). (*F*) Photometry signals were collected from SFR and MS female mice expressing GCaMP6f in the ACC during the SA test. Social interaction bouts are indicated by purple dashes. (*G*) The mean (*Left*) and bar graphs (*Right*) showing that MS females had significantly lower calcium signals during social interaction than SFR females (n = 16 to 17 bouts/4 females/group. Mann–Whitney U-test). (*H*, *Left*) Schematic of in vivo electrophysiological recording of the ACC in freely moving mice. Enlargement depicts the multichannel tetrode. *Right*: the electrode trace in the ACC. (Scale bar: 200 μm). (*I*) Classification of recorded ACC neurons into PNs (black triangles), NFSINs (gray squares), and FSINs (red circles) based on spike waveform and firing rate. *Insets* display typical spike waveforms of a PN and a FSIN, respectively. (*J*, *Left*) Example recording of spontaneous spikes of ACC PN units in a behaving mouse at baseline and during the SA test. Purple lines indicate social interaction epochs. *Middle*: correlation of firing rate at baseline and during social interaction for individual PNs in SFR and MS females. *Insets* displaying proportions of PNs with an increasea decrease, or no change in firing rate during social interaction (n = 91 to 101 units/17 to 19 females/group). *Right*: bar graphs of the change index (CI; [Fi - Fni]/[Fi + Fni]) in the subgroups of SFR (n = 70 units) and MS (n = 17 units) female mice with increased PN units. (*K*, *Left*) Representative immunofluorescent images of c-Fos$^+$ (green) and vGlut1$^+$ (red) neurons in the ACC of SFR and MS mice. Arrowheads indicate colabeled neurons. *Middle*: bar graphs displaying the quantity of c-Fos$^+$ (green) and vGlut1$^+$ (red) neurons in MS females and SFR controls (n = 9 slices/3 females/group. Mann–Whitney U-test). *Right*: bar graphs showing the rate of double-labeled neurons to total vGlut1$^+$ cells (n = 9 slices/3 females/group. Mann–Whitney U-test). (*L*) In vitro whole-cell recordings showing that MS reduced AP firing of ACC PNs compared to SFR controls (n = 5 neurons/3 females/group. Repeated measurement ANOVA). (*M*) MS decreased sEPSC amplitude rather than frequency compared to SFR controls (n = 5 neurons/3 females/group. Two-tailed unpaired *t* test for Amplitude and Mann–Whitney U-test for Frequency). (*N*) PPR was comparable between the SFR group and MS group (n = 5 neurons/3 females/group. Two-tailed unpaired *t* test). Error bars indicate mean ± SEM. **P* < 0.05, ***P* < 0.01. Detailed statistical data are available in *SI Appendix*, Table S3.

lower activity than SFR animals (Fig. 1*E*). After the social stimulus (a control mouse of the same sex and age) was placed beneath the cup, SFR females showed an increase in calcium signal during social interaction epochs (purple lines) (Fig. 1*F*). In contrast to SFR controls, MS females did not exhibit a significant increase in calcium activity over baseline during social interaction epochs (Fig. 1*F*). The perievent averaged calcium signal revealed that SFR mice had considerably increased activity in ACC PNs from the onset of the social interaction, while MS mice exhibited a lower rise in calcium activity (Fig. 1*G*). We found no detectable differences in both the calcium activity and the number of c-Fos$^+$ PNs in the PFC, a brain region also involved in social behavior (16), during the SA test between SFR and MS females (*SI Appendix*, Fig. S5). These data together suggest that MS causes social impairment in female mice, which is linked to the blunted activation of ACC PNs.

We then performed in vivo electrophysiological recordings of ACC neuronal activity in behaving females (Fig. 1*H*). A total of 284 well-isolated units (132 from 17 SFR females, 152 from 19 MS females) were recorded, which were composed of 192 putative PNs (68.0%), 45 fast-spiking interneurons (FSINs; average firing rate >10 Hz), and 47 non-FS INs (NFSINs) (Fig. 1*I* and *SI Appendix*, Fig. S6) (17). We next examined the neuronal activity of ACC PN population at baseline (5 min before the SA test) and during social interaction in SFR and MS females. In the SA assay, SFR mice exhibited a facilitation effect on the mean firing rate of PN units during social engagement epochs compared to baseline (Fig. 1*J*). Quantification of the mean discharge rates during interaction confirmed the above observation as 76.9% of PNs displayed a significant increase in firing rate upon social interaction (Fig. 1*J*). MS female mice, in contrast to SFR females, exhibited fewer PN units (16.8%) that facilitated firing rate and more PN units (SFR: 5.5%; MS: 17.8%) that reduced firing rate during social interaction. Subsequent study of increased PN units indicated that these populations of MS female mice exhibited less firing rate enhancement than SFR females (Fig. 1*J*). However, the majority of recorded INs still maintained their activity during interaction in both SFR and MS females (*SI Appendix*, Fig. S7). Together, these results further indicate that MS causes the hypoactivity of ACC PNs in females during social behavior.

To get a better understanding of ACC PN involvement in social function, we compared the number of c-Fos$^+$ PNs in the ACC of SFR and MS females in the SA test. We found no significant differences in the total number of PNs (vGlut1$^+$ neurons) between SFR and MS mice; what really changed was the number of neurons expressing c-Fos (Fig. 1*K*). Moreover, the coexpression rate of vGlut1 and c-Fos to vGlut1 in MS mice was remarkably less than that in SFR mice (Fig. 1*K*). We next evaluated MS-induced changes in ACC Fos-expressing PNs during a nonsocial test (open-field test). There were no considerable alterations in the number of c-Fos$^+$ PNs between SFR and MS mice (*SI Appendix*, Fig. S8). These results suggest that MS specifically decreases ACC PN activity in social behavior.

To functionally evaluate the hypothesis that MS females regulate PN activity in social behavior, we recorded the firing rate in ACC PNs of SFR and MS females 30 min after the SA test using in vitro whole-cell recordings. Current-clamp recording was used to identify PNs and INs in the ACC as previously described (*SI Appendix*, Fig. S9*A*) (18). Our results showed that MS significantly inhibited the firing rate of PNs (Fig. 1*L*). Given that glutamatergic transmission onto PNs can influence PN activity, we then tested this possibility via in vitro whole-cell recording of ACC PNs in SFR and MS mice. Under this condition, the amplitude of spontaneous excitatory postsynaptic currents (sEPSCs), but not the frequency, was significantly lower in the ACC PNs of MS females than in SFR controls (Fig. 1*M*). To study whether the dysfunction of presynaptic glutamate release onto PNs could contribute to the observed hypoactivity of PNs in MS females, we conducted AMPA receptor-mediated paired-pulse ratio (PPR) to investigate potential alterations in the probability of presynaptic glutamate release. No significant changes were detected in the PPR between SFR and MS mice (Fig. 1*N*), suggesting that MS does not regulate glutamate release onto PNs in the ACC. SFR and MS females did not exhibit significant differences in IN activity (*SI Appendix*, Fig. S9*B*). Summarily, these results indicate that MS-induced social impairment is associated with decreased ACC PN activity.

Activation of ACC PNs Alleviates MS-Induced Social Impairment in Females. To determine whether ACC PNs could play a functional role in the diminished sociability in MS females, we performed optogenetic manipulation of ACC PNs during the SA test. To do this, AAV2/8-CaMKII-hChR2-EYFP was injected into the ACC of MS females, and an optrode was implanted in the ACC (Fig. 2 *A* and *B* and *SI Appendix*, Fig. S10). Under this condition, ACC PNs expressing ChR2 reliably discharged action potentials (APs) in response to photostimulation with 470-nm blue light at 10 Hz (Fig. 2 *C* and *D*). As predicted, 10-Hz photostimulation caused obvious c-Fos expression in the ipsilateral location of virus injection but not in the contralateral site (Fig. 2*E*). SA assay showed that optogenetic activation of ACC in MS females injected with ChR2 in the ACC spent more time interacting with the social stimulus than EYFP controls (Fig. 2 *F* and *G*), without influencing locomotion (*SI Appendix*, Fig. S11*A*). In addition, photoactivation of the PNs in ACC caused an anxiolytic effect in MS females (*SI Appendix*, Fig. S11 *B* and *C*). We also assessed the social interaction time in ChR2-injected MS females triggered by lower (5 Hz) or higher (20 Hz) light stimulation and found that 5 Hz did not alleviate MS-induced diminished sociability, whereas 20 Hz caused a potentiation of social interaction time compared to 10 Hz (*SI Appendix*, Fig. S12).

To activate ACC PNs on an hourly time scale in MS mice, we applied designer receptors that were exclusively activated by designer drug (DREADD) to increase the activity of ACC PNs. To do this, we coinjected AAV2/8-EF1a-DIO-hM3Dq-mCherry and AAV2/8-CaMKII-Cre-EGFP into the ACC of MS females and identified the expression of hM3Dq in ACC PNs (Fig. 2*H* and *SI Appendix*, Fig. S13). Immunostaining and patch-clamp methods confirmed the effectiveness of chemogenetic manipulation (Fig. 2 *I* and *J*). Consistent with the photoactivation-induced beneficial effect on social interaction, injection of clozapine N-oxide (CNO, 3 mg/kg, i.p.) corrected MS-induced social impairment (Fig. 2*K*), without affecting locomotion and anxiety-like behavior (*SI Appendix*, Fig. S14). Given that treatment of CNO has exhibited long-lasting effects over 4 h (19), we recorded the firing rate of ACC PNs from no-DREADDs or hM3Dq mice treated with CNO or saline 30 min after the SA test via in vitro whole-cell recordings. Under this condition, MS-induced reduction of AP firing of ACC PNs was recovered by CNO (Fig. 2*L*). Taken together, these data demonstrate that selective enhancement of ACC PN activity alleviates MS-induced social impairment.

Inhibition of ACC PNs in SFR Females Causes Social Impairment. Next, we evaluated whether photoinhibition of ACC PNs in SFR females would be enough to mimic the social impairment observed in MS females. To do this, the ACC of females was injected with AAV2/8-CaMKIIa-eNpHR3.0-EYFP, and a fiber was implanted in the ACC (Fig. 3*A* and *SI Appendix*, Fig. S15).

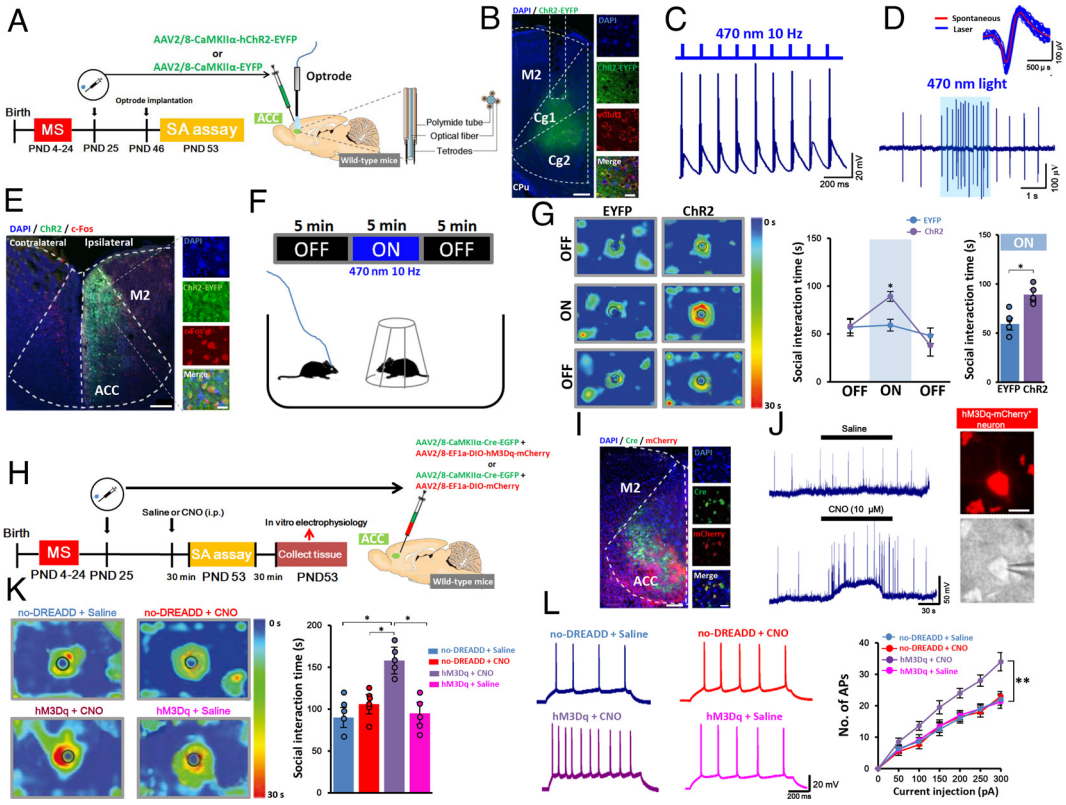

Fig. 2. Optogenetic or chemogenetic activation of ACC PNs ameliorates social impairment in MS females. (*A*) Schematic showing experimental approach and time line for optogenetic activation of ACC PNs in MS females injected with AAV2/8-CaMKIIα-hChR2-EYFP. Magnification showing that optrodes are comprised of a single optical fiber surrounded by multiple tetrodes. (*B*) Typical images of the injection site and unilateral virus-targeted areas within ACC. Enlargement displaying ChR2-expressing neurons colocalized with vGlut1$^+$ neurons. (Scale bars: 200 or 50 μm). (*C*) In vitro whole-cell recordings displaying faithful activation of an ACC PN in response to optogenetic stimulation at 10 Hz. The experiment was conducted five times independently with comparable results. (*D*) A single ACC PN recorded using in vivo optrode recording displayed reliable responses to blue light stimulation at a frequency of 10 Hz. The *Inset* shows the overlay patterns of averaged spontaneous spike waveforms (red) and light-evoked spike waveforms (blue) from the sample unit. The experiment was conducted five times independently with comparable results. (*E*) In the ipsilateral site of ChR2 injection, neurons colocalized with c-Fos-expressing neurons, but not in the contralateral site. (Scale bar: 200 μm). (*F*) Diagram illustrating the SA task and laser delivery approach. (*G*) MS mice injected with ChR2 had longer social interaction times with unfamiliar mice during photoactivation compared to MS mice injected with EYFP (n = 5 females/group. Two-tailed unpaired *t* test). (*H*) Diagram illustrating the experimental process and timetable. A mixture of AAV2/8-EF1a-DIO-hM3Dq-mCherry and AAV2/8-CaMKIIα-Cre-EGFP was infused into the ACC for chemogenetic activation of ACC PNs. (*I*) Representative confocal images showing the virus-targeted areas of the ACC. Enlargement showing hM3Dq-mCherry-expressing neurons colocalized with vGlut1$^+$ neurons. (Scale bars: 200 or 50 μm). (*J*) In a representative neuron expressing hM3Dq-mCherry, bath application of CNO (10 μM) significantly increased the AP firing rate of the hM3Dq-mCherry$^+$ neuron. Inserts showing that hM3Dq-mCherry$^+$ neurons were initially observed using fluorescence and subsequently recorded under infrared differential interference contrast (IR-DIC) video microscopy. (Scale bar: 20 μm). The experiment was conducted five times independently with comparable results. (*K*) Mice expressing hM3Dq-mCherry had longer social interaction times after injection of CNO (3 mg/kg, i.p). (n = 5 to 6 females per group. One-factor ANOVA). (*L*) Mice expressing hM3Dq-mCherry rescued hypoactivity of ACC PNs after injection of CNO (n = 5 neurons/3 females/group. Repeated measurement ANOVA). Error bars indicate mean ± SEM. **P* < 0.05, ***P* < 0.01. Detailed statistical data are available in *SI Appendix*, Table S3.

Under this condition, optogenetic inhibition of ACC PNs in SFR females injected with eNpHR caused social impairment (Fig. 3 *B* and *C*), without affecting locomotion and anxiety-like behavior (*SI Appendix*, Fig. S16). Interestingly, increased sociability was observed in SFR mice injected with ChR2 during optogenetic activation of ACC PNs (*SI Appendix*, Fig. S17 *A* and *B*), and photoactivation of the ACC PNs induced an anxiolytic effect in SFR females (*SI Appendix*, Fig. S17 *D* and *E*), without influencing locomotion (*SI Appendix*, Fig. S17*C*).

To especially silence ACC PNs on a long-term scale, the ACC of SFR mice received the injection of a combination of AAV2/8-EF1a-DIO-hM4Di-mCherry and AAV2/8-CaMKII-Cre-EGFP (Fig. 3 *D* and *E* and *SI Appendix*, Fig. S18). The effectiveness of chemogenetic manipulation was confirmed by a substantial decrease in the number of spikes in tagged ACC PNs following CNO injection (Fig. 3*F*). CNO or saline was injected intraperitoneally into the SFR mice (with hM4Di or no-DREEDR in ACC). As expected, inhibiting ACC PN activity by CNO treatment in SFR females displayed reduced sociability during the SA test (Fig. 3*G*), without altering locomotion and anxiety-like behavior (*SI Appendix*, Fig. S19). In vitro whole-cell recording of slices from saline- or CNO-injected SFR mice (with hM4Di or no-DREEDR in ACC) after the behavior test indicated that the activity of ACC PNs was reduced in MS females injected with CNO + hM4Di (Fig. 3*H*). Taken together, these data provide bidirectional evidence indicating that ACC PNs are causally linked to sociability in females.

MS Down-Regulates Orexin Signaling in ACC of Females. We then explored transcriptome alterations in ACC in MS female mice to better understand how ACC is implicated in MS-induced social dysfunction using RNA-seq analysis. In comparison to SFR controls, we detected 381 down-regulated genes and 427 up-regulated genes in the ACC of MS females (Fig. 4*A*). Heatmaps of the down- and up-regulated genes revealed that SFR samples clustered separately from MS samples (Fig. 4*B*). The RNA-seq functional categorization analysis indicated that down- and up-regulated genes were classified as enzymes, signaling molecules, and transcription factors (Fig. 4*C*). Gene ontology (GO) analysis showed that the down-regulated genes are enriched in

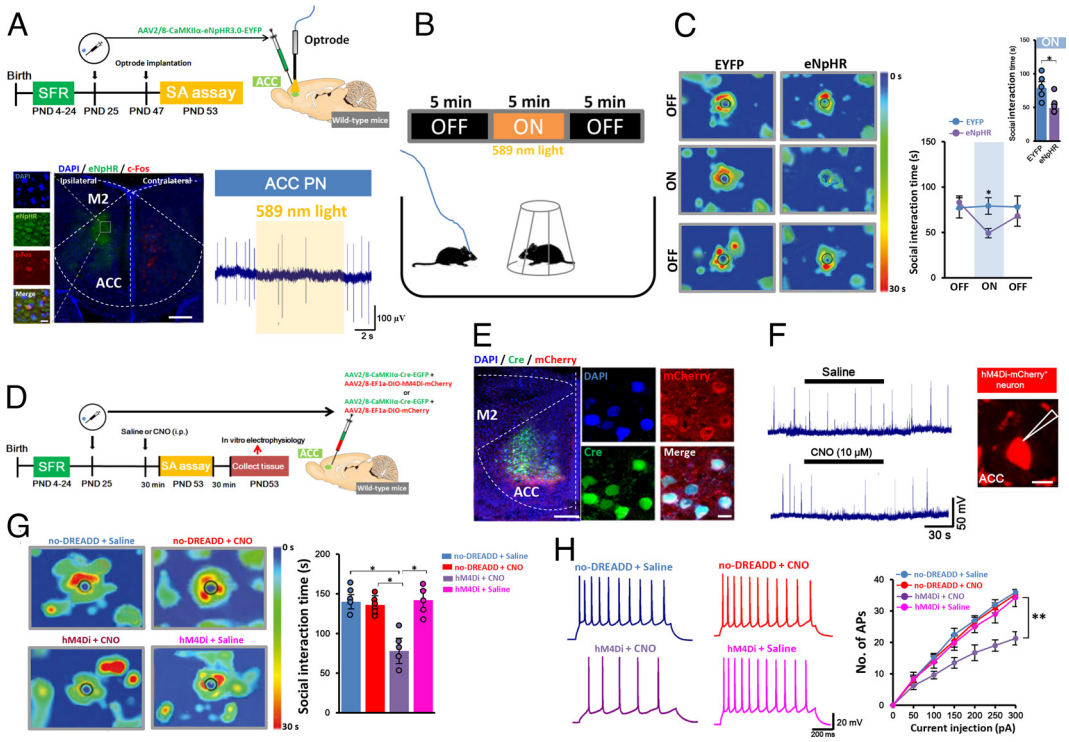

Fig. 3. Optogenetic or chemogenetic inhibition of ACC PNs of SFR females leads to social impairment. (*A*, *Top*) Schematic showing experimental approach and time line for optogenetic inhibition of ACC PNs in SFR females injected with AAV2/8-CaMKIIα-eNpHR3.0-EYFP. *Bottom*: *Left* showing typical images of the injection site and unilateral virus-targeted areas within ACC. (Scale bars: 200 or 20 μm). *Right* showing a sample neuron's reliable responses to yellow light stimulation via in vivo optrode recording. (*B*) Diagram illustrating the SA task and laser delivery approach. (*C*) Mice injected with eNpHR had significantly shorter social interaction time during photoinhibition compared to EYFP-injected mice (n = 5 females/group. Mann–Whitney U-test). (*D*) Schematic showing experimental approach and time line. The ACC was injected with a combination of AAV2/8-EF1a-DIO-hM4Di-mCherry and AAV2/8-CaMKIIα-Cre-EGFP for chemogenetic inhibition of ACC PNs. (*E*) Representative confocal images showing the unilateral virus-targeted areas of the ACC. Enlargement showing hM4Di-mCherry^{+} neurons colocalized with vGlut1^{+} neurons. (Scale bars: 200 or 20 μm). (*F*) In a representative neuron expressing hM4Di-mCherry, application of CNO markedly reduced the AP firing rate of the identified hM3Dq-mCherry^{+} neuron. (Scale bar: 20 μm). The experiment was conducted five times independently with comparable results. (*G*) Mice expressing hM4Di-mCherry had shorter social interaction time after intraperitoneal injection of CNO (n = 5 to 6 females/group. One-factor ANOVA). (*H*) Mice expressing hM4Di-mCherry caused hypoactivity in ACC PNs of SFR mice after injection of CNO (n = 5 neurons/3 females/group. Repeated measurement ANOVA). Error bars indicate mean ± SEM. **P* < 0.05, ***P* < 0.01. Detailed statistical data are available in *SI Appendix*, Table S3.

"neuropeptide signaling pathway", and the up-regulated genes are enriched in "receptor/signaling molecule" (Fig. 4*D*). The neuropeptide signaling system has been reported to link with stress responses (20) and female-biased mental disease including depression (21). Hcrt and Pomc, two neuropeptide genes, were identified as the "hubs" linking with other high-ranking down-regulated genes in a protein–protein interaction (PPI) network (Fig. 4*E*). Moreover, the decrease of Hcrt and Pomc mRNAs in the ACC of MS females was confirmed by quantitative PCR (Fig. 4*F*). Hcrt, the most down-regulated gene in the ACC of MS female mice, encodes hypocretin (orexin), a neuropeptide that affects wakefulness, arousal, and endocrine homeostasis (22). We next assessed orexin concentration in the ACC of MS female mice after the SA test using an enzyme-linked immunosorbent assay (ELISA). We found a significant decrease in orexin levels in the ACC of MS mice compared to SFR mice (Fig. 4*G*).

Orexin receptor-1 (OxR1) and orexin receptor-2 (OxR2), which are two orexin receptor subtypes, are known to mediate orexin functions (23, 24). We then characterized the expression pattern of OxR1 and OxR2 in PNs and INs of ACC in SFR mice; approximately 30% of PNs and 20% of INs were positive for OxR1 (*SI Appendix*, Fig. S20*A*). Interestingly, we found OxR2 expression in more than 90% of ACC PNs but only in less than 20% of ACC INs (*SI Appendix*, Fig. S20*B*). We also found that many orexin fibers were close to cell bodies of ACC PNs (*SI Appendix*, Fig. S20*C*). Quantitative PCR revealed a significant reduction of OxR2 rather than OxR1 mRNA levels in the ACC of MS females, compared to SFR controls (Fig. 4*H* and *SI Appendix*, Fig. S21). Using immunohistochemical analysis, decreased OxR2 expression was also observed in ACC PNs, but not INs, of MS females (Fig. 4 *I* and *J*). However, MS did not influence OxR1 expression in both PNs and INs of the ACC (*SI Appendix*, Fig. S22). Together, these results suggest that MS-induced social impairment is related to alterations in the OxR2 signaling in ACC PNs.

Activation of Orexin Signaling in the ACC Ameliorates MS-Induced Social Impairment. To functionally test whether orexin could modulate ACC PN activity, brain slice electrophysiology was performed with CaMKII-, Pvalb-, or Sst-tdTomato mice, respectively. Orexin-A (100 nM) was applied to these neurons in ACC slices under whole-cell voltage clamp. We found that orexin-A (100 nM) increased the firing rate of PNs without regulating the activity of Sst or Pvalb interneurons (Fig. 5 *A*–*C*), indicating that PNs rather than INs are physiologically activated by orexin.

Given that cell bodies of orexin neurons are exclusively observed in the lateral hypothalamus (LH) (25), we then tested whether photoactivation of the LH to ACC orexin projections could increase the activity of PNs in MS mice. To do this, we optogenetically activated ACC orexin terminals in orexin-Cre females receiving the injection of AAV1-hSyn-DIO-ChR2-EYFP within LH (Fig. 5*D* and *SI Appendix*, Fig. S23). Photoactivation of ACC orexin terminals was indicated to increase ACC PN firing rate via

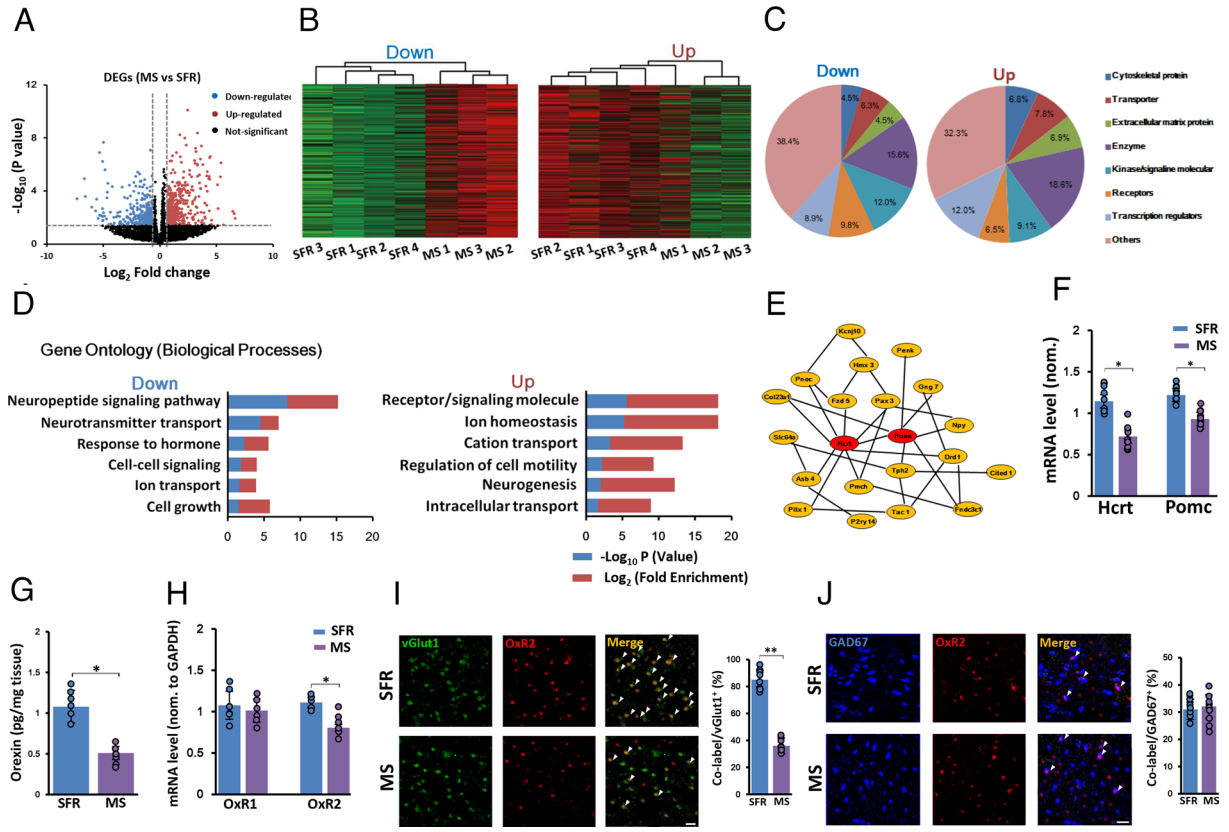

Fig. 4. MS down-regulates orexin signaling in ACC. (*A*) Transcriptomic studies revealed a volcano plot based on gene expression levels in MS female mice vs SFR female mice. Tan dots represented up-regulated genes, blue dots represented down-regulated genes, and black dots represented genes that remained unaltered. (*B*) Heatmaps representing expression of up- and down-regulated genes in ACC from MS female mice relative to SFR females. (*C*) Analysis of the up- and down-regulated genes' functional protein categorization. (*D*) Gene ontology (GO) biological process analysis of up- and down-regulated genes. (*E*) Protein–protein interaction (PPI) network of the top down-regulated genes in the ACC of MS female mice. PPI network hub genes included Hcrt and Pomc, which encode neuropeptides. (*F*) The mRNA level of Hcrt (n = 9 slices/3 females/group. Two-tailed unpaired *t* test) and Pomc (n = 9 slices/3 females/group. Two-tailed unpaired *t* test) as determined by quantitative PCR in the ACC of SFR and MS females. (*G*) ELISA analyses showing orexin level in ACC of SFR and MS females (n = 6 slices/3 females/group. Two-tailed unpaired *t* test). (*H*) The mRNA level of OxR1 (n = 6 slices/3 females/group. Two-tailed unpaired *t* test) and OxR2 (n = 6 slices/3 females/group. Two-tailed unpaired *t* test) in the ACC of SFR and MS females. (*I* and *J*) Representative confocal images and bar graphs showing that MS decreased OxR2 (red) expression in ACC vGlut1$^+$ neurons (green) (n = 9 slices/3 females/group. Two-tailed unpaired *t* test) (*I*), without affecting OxR2 expression in GAD 67$^+$ interneurons (blue) (n = 9 slices/3 females/group. Two-tailed unpaired *t* test) (*J*). Arrowheads indicate colabeled neurons. (Scale bar: 50 μm). Error bars indicate mean ± SEM. *P < 0.05, **P < 0.01. Detailed statistical data are available in *SI Appendix*, Table S3.

in vivo multitetrode recordings of freely moving females (Fig. 5*E*). Staining with c-Fos was used to further assess the effect of optogenetic manipulations on PN activity in the ACC after mice were stimulated with blue light for 10 min. Under this condition, photostimulation of ACC orexin terminals increased c-Fos expression in ACC PNs of MS females compared to females injected with EYFP (Fig. 5*F*). In the SA test, photoactivation of ACC orexin terminals in MS orexin-Cre females injected with ChR2 exhibited longer social interaction time compared to mice received the injection of EYFP (Fig. 5*G*), without modulating locomotion and anxiety-like behavior (*SI Appendix*, Fig. S24). To confirm the role of OxR2, photoactivation of ACC orexin terminals was conducted in MS orexin-Cre mice expressing an anti-OxR2 microRNA (AAV-miR-OxR2) in the ACC. Under this condition, stimulation of ACC orexin terminals did not increase social interaction time (*SI Appendix*, Fig. S25).

To activate ACC orexin terminals on a long-term scale, we injected AAV-retro-hSyn-DIO- hM3Dq-mCherry into the ACC of orexin-Cre females (Fig. 5*H* and *SI Appendix*, Fig. S26). Immunostaining and patch-clamp experiments were performed to confirm the effectiveness of chemogenetic manipulation (Fig. 5 *H* and *I*). Consistent with the results from the optogenetic activation approach, activating orexin terminals in the ACC by treatments of CNO increased social interaction time compared to MS mice injected with no-DREADD control (Fig. 5*J*), without influencing locomotion and anxiety-like behavior (*SI Appendix*, Fig. S27). After the SA test, we performed immunostaining for c-Fos and vGlut1. Elevated c-Fos expression in vGlut1$^+$ neurons was observed in MS females (with hM3Dq in ACC) by treatment of CNO (Fig. 5*K*). We also conducted in vitro whole-cell recordings of ACC PNs from MS females (with no-DREADD or hM3Dq in ACC) injected with CNO or saline 30 min after the SA test. Under this condition, MS-induced reduction of AP firing and sEPSC amplitude of ACC PNs in MS females were restored by CNO treatment (Fig. 5 *L* and *M*). Again, no significant differences were detected in the PPR between groups (Fig. 5*N*). These results collectively suggest that activation of orexin signaling in the ACC alleviates social impairment and rescues the hypoactivity of PNs observed in MS females.

Inhibition of Orexin Signaling in the ACC of SFR Females Mimics Hypoactivity of PNs and Social Impairment Observed in MS Females. We then tested whether inhibition of orexin projections from LH to ACC in SFR females could mimic the hypoactivity of PNs observed in MS females, we optogenetically inhibited ACC orexin terminals in orexin-Cre females receiving the injection of AAV1-hSyn-DIO-eNpHR-EYFP within LH (Fig. 6*A* and *SI Appendix*, Fig. S28). Under this condition, photoinhibition of

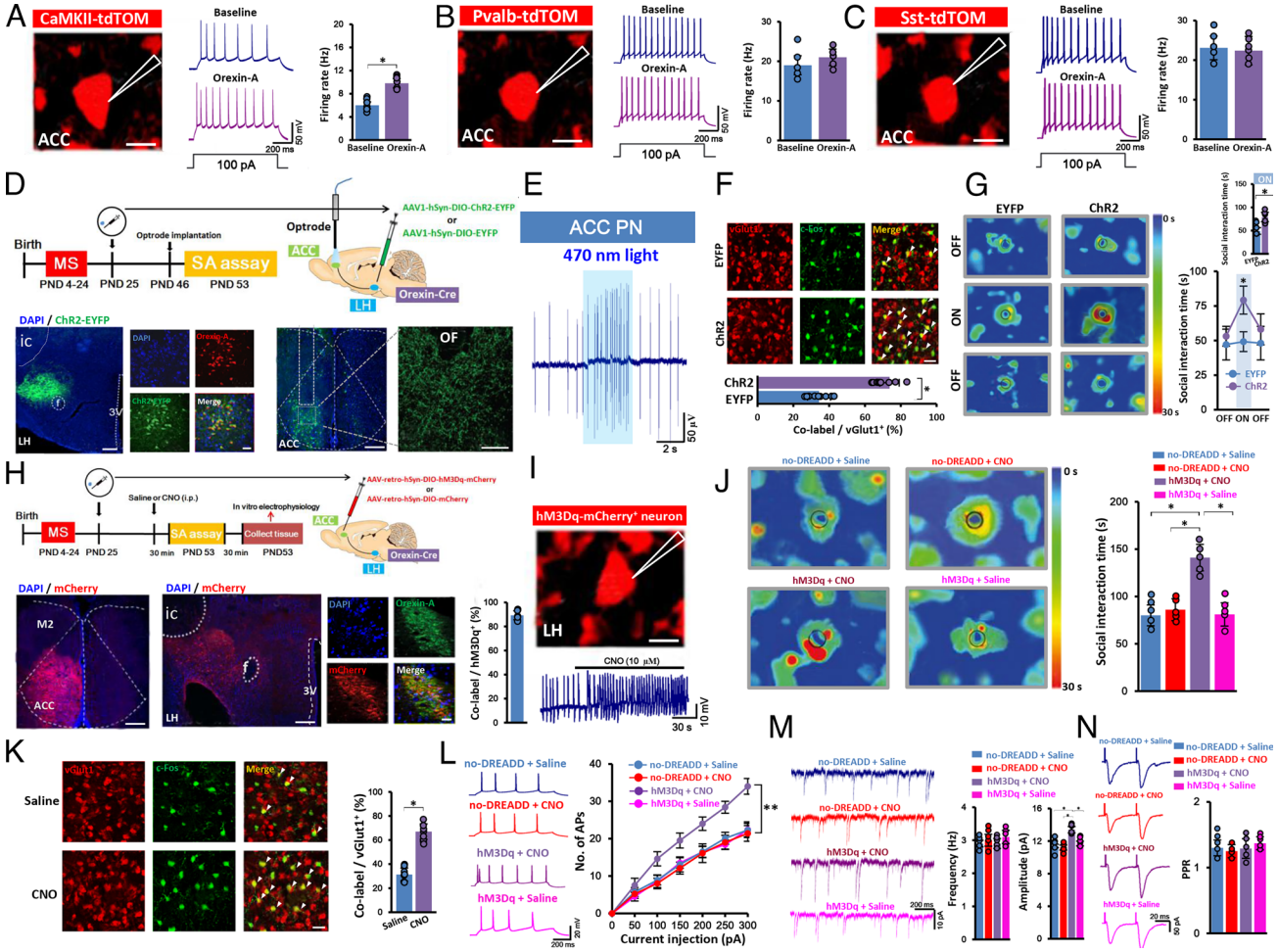

Fig. 5. Optogenetic or chemogenetic activation of orexin signaling in the ACC of MS females rescues hypoactivity of PNs and ameliorates social impairment. (*A*, *Left*) A representative image of PNs with whole-cell recording from a CaMKII-tdTOM mouse. *Right*: sample traces and statistical data for AP firing recorded from tdTOM-expressing neurons before and during orexin-A (100 nM) application (n = 6 neurons/3 females. Two-tailed paired *t* test). (*B* and *C*) Representative images of Pvalb (*B*) and Sst (*C*) interneurons from Pvalb-tdTOM and Sst-tdTOM mice. Sample traces and statistical data showing that application of orexin-A (100 nM) did not affect the AP firing rate of Pvalb and Sst interneurons (Pvalb-tdTOM: n = 5 neurons/3 females. Sst-tdTOM: n = 5 neurons/3 females. Two-tailed paired *t* test). (*D*, *Top*) Schematic showing the experimental approach and time line for optogenetic activation of ACC orexin terminals in orexin-Cre mice received the injection of AAV1-hSyn-DIO-ChR2- EYFP. *Bottom*: *Left* showing typical images of the virus-targeted areas within LH. *Insets* showing ChR2-expressing neurons colocalized with orexin neurons. *Right* showing representative viral infections of ChR2 in the ACC and optical-fiber site. (Scale bars: 200 or 50 μm). LH, lateral hypothalamic; ic, internal capsule; f, fornix; OF, the tip of the optic fiber. (*E*) Sample traces showing optrode recordings of firing rate of a PN in MS orexin-Cre females with ACC injection of ChR2 before, during, and after 10-Hz photoactivation with a 470-nm laser. (*F*) Representative confocal images and data of c-Fos$^+$ PNs in the ACC of MS orexin-Cre females with ACC injection of ChR2 or EYFP after 10-min blue light photostimulation (n = 9 slices/3 females/group. Two-tailed unpaired *t* test). Arrowheads indicate colabeled neurons. (Scale bar: 50 μm). (*G*) MS orexin-Cre mice injected with ChR2 had significantly longer social interaction time during photostimulation (n = 5 females/group. Two-tailed unpaired *t* test). (*H*, *Top*) Schematic showing experimental approach and time line for chemogenetic activation of orexin terminals in the ACC. AAV-retro-hSyn-DIO-hM3Dq-mCherry was injected into the ACC of orexin-Cre mice for chemogenetic activation of ACC orexin terminals. *Bottom*: typical images showing the unilateral virus-targeted areas of the ACC (*Left*). An example coronal image showing that virus injection in the ACC resulted in the expression of hM3Dq-mCherry (red) in the ACC-projecting orexin neurons in the LH. Enlargement showing nearly 100% hM3Dq-mCherry-expressing neurons colocalized with orexin-A$^+$ neurons in the LH (*Middle*). *Right* showing the percentage of colabeled neurons in all hM3Dq$^+$ neurons (92.4 ± 4.1%) of the LH after the virus infections (n = 5 mice). (Scale bars: 200 or 50 μm). (*I*) Patch-clamp recordings were performed on the hM3Dq-mCherry$^+$ LH orexin neuron after 3 wk of the virus injections in the brain slices. A 2-min CNO application enhanced the firing rate in all six identified hM4Di-mCherry$^+$ LH orexin neurons. (Scale bar: 20 μm). (*J*) MS orexin-Cre mice expressing hM3Dq-mCherry had longer social interaction time after injection of CNO (n = 5 females/group. One-factor ANOVA). (*K*) Typical images and data of c-Fos$^+$ PNs in the ACC from saline- or CNO-injected MS orexin-Cre mice (with hM3Dq in ACC) (n = 9 slices/3 females/group. Two-tailed unpaired *t* test). Arrowheads indicate colabeled neurons. (Scale bar: 50 μm). (*L*–*N*) Representative traces of APs (*L*), sEPSC (*M*) or PPR (*N*) of ACC PNs from saline- or CNO-injected MS orexin-Cre mice (with hM3Dq or no-DREADD in ACC). Summary data showing that MS orexin-Cre mice expressing hM3Dq-mCherry enhanced AP firing (*L*) and sEPSC amplitude (*M*) without altering sEPSC frequency (*M*) and PPR (*N*) of ACC PNs after injection of CNO (n = 5 neurons/3 females/group. Repeated measurement ANOVA or one-factor ANOVA). Error bars indicate mean ± SEM. **P* < 0.05, ***P* < 0.01. Detailed statistical data are available in *SI Appendix*, Table S3.

ACC orexin terminals decreased the firing of ACC PN in freely moving mice (Fig. 6*B*). In addition, the immunostaining assay indicated that optogenetic inhibition of orexin terminals in the ACC for 10 min reduced c-Fos expression in vGlut1$^+$ neurons (Fig. 6*C*). In the SA test, photoinhibition of ACC orexin terminals in SFR orexin-Cre females received the injection of eNpHR decreased social interaction time compared to mice received the injection of EYFP (Fig. 6*D*), without altering locomotion and anxiety-like behavior (*SI Appendix*, Fig. S29). To inhibit ACC orexin terminals on a long-term scale, we injected AAV-retro-hSyn-DIO -hM4Di- mCherry into the ACC of SFR orexin-Cre mice and verified the effectiveness of chemogenetic manipulation (Fig. 6 *E* and *F* and *SI Appendix*, Fig. S30). As expected, administration of CNO decreased social interaction time in SFR mice injected with hM4Di in the ACC (Fig. 6*G*), without affecting locomotion and anxiety-like behavior (*SI Appendix*, Fig. S31).

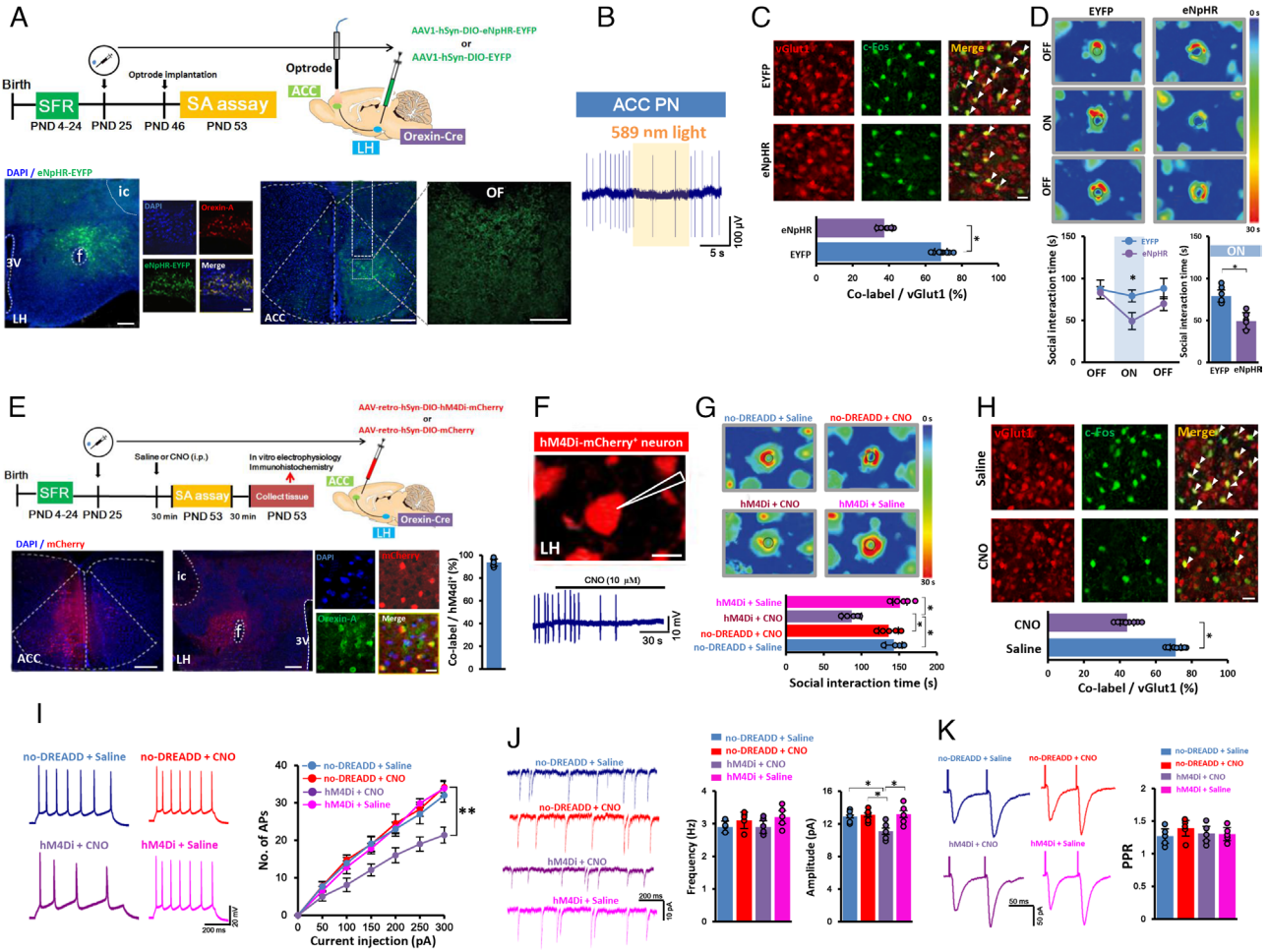

Fig. 6. Optogenetic or chemogenetic inhibition of orexin signaling in the ACC of SFR females leads to hypoactivity of ACC PNs and social impairment. (*A*, *Top*) Schematic showing the experimental approach and time line for optogenetic inhibition of ACC orexin terminals in orexin-Cre females received the injection of AAV1-hSyn-DIO-eNpHR- EYFP. *Bottom*: *Left* showing typical images of the virus-targeted areas within LH. Enlargement showing eNpHR-expressing neurons colocalized with orexin neurons. *Right* showing representative viral infections of eNpHR in the ACC and location of optical-fiber in the ACC. (Scale bars: 200 or 50 μm). (*B*) Sample traces showing optrode recordings of a representative PN firing rate in SFR orexin-Cre mice injected with eNpHR before, during, and after photoinhibition with a 589-nm laser. (*C*) Representative images and data of c-Fos$^+$ PNs in the ACC of SFR orexin-Cre females received the injection of eNpHR or EYFP after 10-min light photoinhibition (n = 9 slices/3 females/group. Two-tailed unpaired *t* test). Arrowheads indicate colabeled neurons. (Scale bar: 50 μm). (*D*) SFR orexin-Cre mice injected with eNpHR had shorter social interaction time during photoinhibition compared to orexin-Cre mice injected with EYFP (n = 5 females/group. Two-tailed unpaired *t* -test). (*E*, *Top*) Diagram illustrating the experimental procedure and time line. AAV-retro-hSyn- DIO-hM4Di-mCherry was delivered into the ACC of SFR orexin-Cre females for chemogenetic inhibition of ACC orexin terminals. *Bottom*: a representative image showing the unilateral virus-targeted areas of the ACC (*Left*). *Middle* showing that virus injection in the ACC resulted in the expression of hM4Di-mCherry (red) in the ACC-projecting orexin neurons in the LH. Enlargement shows nearly 100% hM4Di-mCherry-expressing neurons colocalized with orexin-A$^+$ neurons. *Right* showing the percentage of co-labeled neurons in all hM4Di$^+$ neurons (93.7 ± 3.1%) after the virus infections (n = 5 mice). (Scale bars: 200 or 50 μm). (*F*) A 2-min CNO application significantly reduced the firing rate in all five identified hM4Di-mCherry$^+$ LH orexin neurons. (Scale bar: 20 μm). (*G*) SFR orexin-Cre mice expressing hM4Di-mCherry had shorter interaction time after injection of CNO (n = 5 females/group. One-factor ANOVA). (*H*) Typical images and data of c-Fos$^+$ PNs in the ACC from saline- or CNO-injected SFR orexin-Cre mice (with hM4Di in ACC) (n = 9 slices/3 females/group. Two-tailed unpaired *t* test). Arrowheads indicate co-labeled neurons. (Scale bar: 50 μm). (*I-K*) SFR orexin-Cre mice expressing hM4Di-mCherry caused hypoactivity of PNs (*I*) and decrease of sEPSC amplitude (*J*), without altering sEPSC frequency (*J*) and PPR (*K*) after injection of CNO (n = 5 neurons/3 females/group. Repeated measurement ANOVAone-factor ANOVA or Kruskal–Wallis H-test with the Nemenyi multiple comparisons test). Error bars indicate mean ± SEM. **P* < 0.05, ***P* < 0.01. Detailed statistical data are available in *SI Appendix*, Table S3.

Post hoc immunostaining showed a considerable reduction of c-Fos expression in ACC PNs of SFR females (with hM4Di in ACC) by treatment of CNO (Fig. 6*H*). We also examined the excitability of ACC PNs from no-DREADD or hM4Di mice injected with CNO or saline using in vitro whole-cell recordings. Under this condition, hM4Di mice injected with CNO reduced AP firing and sEPSC amplitude of ACC PNs, without modulating sEPSC frequency and PPR (Fig. 6 *I–K*). These results together demonstrate that inhibition of ACC orexin signaling in SFR mice is capable of mimicking the hypoactivity of PNs as well as the social impairment observed in MS females.

Knockdown of OxR2 in ACC PNs Causes Social Impairment in SFR Females, Whereas Overexpression of OxR2 in ACC PNs Ameliorates Social Deficit in MS Females. We then investigated whether pharmacological inhibition of OxR2 would cause the diminished sociability in SFR females. EMPA, an OxR2 antagonist, was intraperitoneally injected (30 mg/kg) into SFR females. Under this condition, we observed a reduction of social interaction time compared with vehicle controls, without changes in locomotion and anxiety-like behavior (*SI Appendix*, Fig. S32). To further assess whether OxR2 signaling in ACC PNs was involved in social behavior, we conducted PN-specific knockdown of OxR2 in the ACC of SFR mice using a microRNA-based approach. To do this, we bilaterally injected AAV2-EF1a-DIO-miR-OxR2-GFP or AAV2-EF1a-DIO-miR-scrambled-GFP into the ACC of CaMKIIα-Cre mice, and verified the effectiveness of virus (Fig. 7 *A* and *B* and *SI Appendix*, Fig. S33). We found that knockdown of OxR2 in ACC

PNs of MS females decreased social interaction time compared to females received the injection of scrambled control (Fig. 7*C*), without influencing locomotion and anxiety-like behavior (*SI Appendix*, Fig. S34). Given that MS reduces the OxR2 expression in ACC PNs, we next examined whether overexpression of OxR2 in ACC PNs would be sufficient to rescue MS-induced social impairment via bilaterally injecting AAV2-EF1a-DIO-OxR2-GFP or AAV2-EF1a-DIO-GFP into the ACC of CaMKIIα-Cre mice (Fig. 7 *D* and *E* and *SI Appendix*, Fig. S35). As expected, MS CaMKIIα-Cre females received the injection of AAV-OxR2 within ACC had longer social interaction time with social stimulus compared to mice received the injection of GFP control (Fig. 7*F*), without influencing locomotion and anxiety-like behavior (*SI Appendix*, Fig. S36). Summarily, these results support the notion that OxR2 signaling in ACC PNs contributes to social impairment induced by MS.

Discussion

In the current research, we employed MS, a classic early-life stress model, for investigating the potential neurobiology of social ability. Our data indicate a causal link between the diminished sociability and the hypoactivity of ACC PNs in MS females. More importantly, we found that after 3 wk of postweaning MS females caused dysfunction of the endogenous orexin system, decreased orexin inputs to the ACC resulted in hypoactivity of ACC PNs and social impairment via an OxR2-dependent mechanism.

The role of ACC in social functions in humans and animals has been highlighted (12, 21). Besides ACC, PFC is another crucial region involved in social behaviors (16). Recently, a study from Xu et al. revealed that activation of PFC caused social fear (26), whereas our findings revealed that excitation of ACC improved social interaction. These contradicting findings suggest that the PFC and ACC may play different roles in social behavior. In addition, it should be noted the lack of consensus on anatomical definitions of ACC and PFC. For example, the prelimbic cortex (which is almost entirely equivalent to area 32) and infralimbic cortex (equivalent to area 25), which are considered as part of the ACC utilizing the ACC/MCC definition in mammals such as rabbits, primates, and humans, are not part of either Cg1 or Cg2, but are treated as subregions of PFC in rats and mice using the Cg1/Cg2 nomenclature (7). The precise mechanisms by which the PFC and ACC affect social functions may be better understood by further studies examining the distinct subregions and cell types in the PFC and ACC and their functional connections using real-time, functional imaging of live neurons.

In this study, photoactivation of the ACC PNs has an anxiolytic effect in addition to improving social function. Indeed, ACC has been found to be connected with anxiety (27), and a human study has indicated a possible relationship between anxiety and social difficulties (28). Therefore, it is reasonable to presume that these two behavioral phenotypes may share underlying neural mechanisms, at least in part. However, we found that photoinhibition of ACC PNs did not alter anxiety-like behavior, consistent with a report revealing that selective inhibition of PN activity in the ACC does not influence anxiety induced by inflammatory pain (29). Therefore, our present results suggest that ACC unidirectionally modulates anxiety-like behavior. One possible explanation is that anxiety is not regulated by a normal physical change in ACC activity. When the activity of the ACC reaches a specific level in the brain, for example, 10 Hz photostimulation of PNs in the current experimental situation, it results in an anxiolytic effect. It is worth noting that a higher frequency of photoactivation (20 Hz) seems to have better benefits than a lower frequency, but if the stimulation goes beyond the normal range of ACC neuronal activity, the excitatory/inhibitory balance could be disrupted, leading to different results.

Our RNAseq analysis revealed that Hcrt was the top-ranking down-regulated gene in the ACC of MS females. Orexin is produced by the cleavage of prepro-orexin, which is encoded on the Hcrt gene. Note that the LH is the sole brain region where the neuropeptide orexin is synthesized (25). Orexin neuron cell bodies are located solely in the LH, but project to many regions and modulate multiple complex behaviors, including sleep/wakefulness, feeding, aggression, and cognition (30–33). Here, our results show that activating ACC orexin signaling mitigates MS-induced

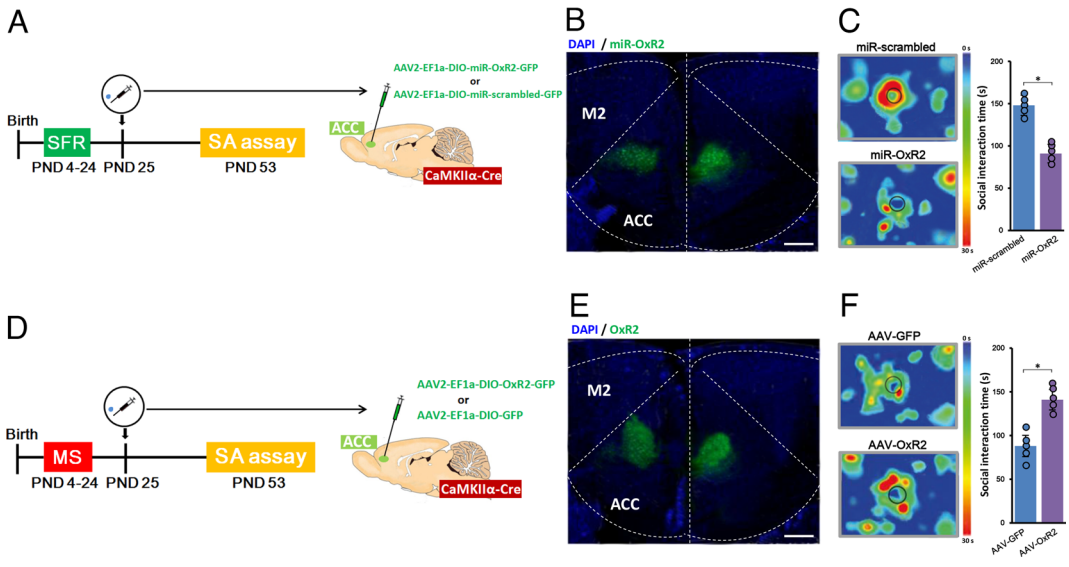

Fig. 7. Knockdown of OxR2 in ACC PNs of SFR females causes social impairment, whereas overexpression of OxR2 in ACC PNs of MS females ameliorates social impairment. (*A*) Schematic showing the experimental approach and time line. AAV2-EF1a-DIO-miR-OxR2-GFP was injected into the ACC of SFR CaMKIIα-Cre mice for PN-specific knockdown of ACC OxR2. (*B*) Typical viral infection for PN-specific silencing of OxR2 in the ACC of SFR CaMKIIα-Cre mice. (Scale bar: 200 μm). (*C*) SFR CaMKIIα-Cre mice expressing miR-OxR2 had shorter social interaction time compared to mice injected with miR-scrambled (n = 5 females/group. Two-tailed unpaired *t* test). (*D*) Diagram illustrating the experimental procedure and time line. AAV2-EF1a-DIO-OxR2-GFP was injected into the ACC of MS CaMKIIα-Cre mice for PN-specific overexpression of OxR2 in the ACC. (*E*) Typical viral infection for PN-specific OxR2 overexpression in the ACC of MS females. (Scale bar: 200 μm). (*F*) MS CaMKIIα-Cre mice expressing AAV-OxR2 had longer social interaction time compared to GFP-mice (n = 5 females/group. Two-tailed unpaired *t* test). Error bars indicate mean ± SEM. $^*P < 0.05$. Detailed statistical data are available in *SI Appendix*, Table S3.

social impairment, indicating orexin as a potential therapeutic target for improving social deficits induced by early-life stress in females. Interestingly, we found MS females were more vulnerable to developing social impairment compared to males. In orexin research, sex differences have been repeatedly reported so far. For example, orexin has been found to mediate sex differences in expression pattern, stress response as well as cognitive flexibility (34–36). It is worth further investigating whether and how orexin signaling regulates MS-induced changes in social function in a sex-dependent manner. Considering that the orexin system is implicated in feeding behavior, we were surprised to find that MS did not alter food intake in our study. The possible explanation is that the LH to ACC orexin projections are not required for feeding behavior. Instead, LH orexin neurons predominantly modulate feeding behavior through projections to brain regions outside the ACC, such as the ventral tegmental area (VTA) (37).

Our work presents evidence that orexin signaling modulates the activity of PNs in the ACC. Nonetheless, many issues remain concerning orexin neurons. First, besides orexin, do orexin neurons release other neurotransmitter (s)? Notably, the activation of orexin neurons did not result in the release of glutamate onto ACC PNs because chemogenetic activation of orexin neurons did not alter sEPSC frequency and PPR, both of which are classical electrophysiological measurements representing alterations in glutamate release. However, it is still possible that orexin neurons release additional messengers. Actually, orexin neurons release not only orexins but also dynorphin (38) and serotonin (5-HT) (39), which are all implicated in stress-related disorders. It is worth investigating whether orexin neurons influence ACC PN activity via modulating other neurotransmitters besides orexin and, second, besides ACC, whether orexin neurons projecting to other brain regions are essential for social deficits. Notably, LH provides a top-down modulating signal to the VTA, a brain area associated with the regulation of social behaviors (40). An optogenetic study has revealed that enhanced phasic firing of VTA dopaminergic (DA) neurons mediates susceptibility to social defeat stress (41). It is possible that projections from LH to VTA may regulate the burst firing of DA neurons. Future studies should test whether orexin neurons projections from LH to other brain regions besides ACC also mediate MS-induced social impairment. Third, besides orexin input, are other inputs to ACC PNs implicated in MS-induced social impairment? In addition to expressing OxR2, ACC PNs also express oxytocin and μopioid receptor, both of which have been linked to social function (42, 43). This should also be investigated in future studies. In addition to receiving projections from LH, ACC also send glutamatergic projections to the lateral habenula, which inhibits social approach behavior in adult rats (44). Considering the important role of ACC PNs in social behavior after early-life adversity, it is worth exploring further in the future whether alteration in the projections from ACC PNs to the lateral habenula contributes to the diminished sociability induced by MS.

In this study, we found that intraperitoneal injection of the OxR2 antagonist EMPA caused the diminished sociability, without influencing locomotor behavior. The absence of an impact of EMPA on locomotion is somewhat unexpected because orexin signaling is integral for promoting wakefulness. Indeed, it has been reported that brain-wide deletion of OxR2 leads to narcolepsy-like phenotypes (45). Moreover, suvorexant, a dual orexin receptor antagonist, is widely used for the treatment of insomnia (46). Whereas a prior study demonstrated that intraperitoneal injection of 30 mg/kg EMPA could decrease spontaneous locomotion in rats (47), it had no effect on locomotion in mice (48). It is possible that, at low doses, EMPA may cause social deficits without affecting arousal. However, considering that spontaneous locomotion is not an extremely sensitive measure of arousal, future studies should examine this possibility more thoroughly.

Overall, our study demonstrates an indispensable role for the ACC orexin system in MS-induced social impairment in females. Activation of orexin input from the LH to the ACC rescues MS-induced social impairment via an OxR2-dependent mechanism. These results not only point to a potential neural circuit responsible for MS-induced social impairment, but also provide a perspective on the treatment of social behavior dysfunction in neuropsychiatric disorders induced by early-life stress in females.

Materials and Methods

Animals. All experiments were performed with the approval of the Institutional Animal Care and Use Committee of Nanchang University and in accordance with the NIH guidelines. C57BL/6J wild-type mice, orexin-Cre mice, and CaMKIIα-Cre mice were used for experiments. Mice were housed in a 12-h light–dark cycle (lights on from 8:00 a.m.to 8:00 p.m.) with water and food available ad libitum. The temperature was maintained at 25 ± 1 °C, and the humidity was controlled between 40% and 60%. See *SI Appendix* for details.

Early-Life Stress. Briefly, postnatal stress was applied for 21 d from PND 4 to 24. Pups were removed from the cage, placed in a clean plastic cage for 3 h per day (*SI Appendix*, Table S1), and returned to their home cages 3 h later. See *SI Appendix* for details.

Behavior Tests. The social approach test, open-field test, elevated plus maze test, or feeding behavior test was employed to examine sociability, locomotion, anxiety-like behavior, or food intake, respectively. See *SI Appendix* for details.

Surgery and Virus Injection. Mice were given an intraperitoneal injection of sodium pentobarbital (30 mg/kg), and then placed on a stereotaxic device (RWD). Viruses were injected bilaterally for behavioral manipulation and unilaterally for fiber photometry, optogenetic or chemogenetic manipulation. See *SI Appendix* for details.

Behavioral Pharmacology. Mice were given an intraperitoneal injection of either 30 mg/kg EMPA or vehicle 30 min before the behavioral test. See *SI Appendix* for details.

In Vivo Calcium Imaging of Behaving Animals. AAV1-CaMKII-GCaMP6f virus was delivered into the brain regions of interest. After 3 wk, an optical fiber was surgically implanted in the brain areas to capture calcium signals in behaving mice. See *SI Appendix* for details.

Surgical Implantation of Tetrodes. After a craniotomy was done and the dura mater was removed, an array including eight tetrodes was inserted into the ACC to record electrophysiological signals in behaving animals. See *SI Appendix* for details.

In Vivo Optogenetic Manipulations. For in vivo optogenetic tagging of ACC PNs or orexin terminals, WT mice or orexin-Cre mice were unilaterally delivered with AAV2/8-CaMKIIα-hChR2-EYFP into the ACC or AAV1-hSyn-DIO-ChR2-EYFP into the LH. See *SI Appendix* for details.

In Vivo Electrophysiology during SA Test. Electrical signals were digitized at 30 kHz and recorded with a neural data acquisition system (Blackrock Microsystems) throughout the behavioral test. See *SI Appendix* for details.

Spike Sorting, Unit Classification and Firing Rate Analysis. Neuronal signals were amplified, filtered at a 300 to 5,000-Hz bandwidth, and stored using Offline Spike Sorter software (Plexon Inc.). The well-isolated units were first classified into the wide-spiking putative PNs, narrow-spiking INs (FS-IN), and nonfast spike INs (NFS-IN) based on the k-means method and baseline firing rate. See *SI Appendix* for details.

Chemogenetic Manipulations. The virus was delivered unilaterally to the ACC of females. After at least 3 wk of virus expression, the SA test was conducted 30 min after intraperitoneal injection of CNO or saline in viral-infected mice. See *SI Appendix* for details.

Immunohistochemistry and ISH (in situ hybridization). For immunohistochemistry experiments, sections with ACC were labeled with primary antibodies against rabbit anti-c-Fos (1:1000, Millipore, Cat# ABE457), goat anti-orexin-A (1:500, Santa Cruz, Cat# sc8070), rabbit anti OxR1 antibody (1:100, Abcam, Cat# ab68718), goat anti OxR2 antibody (1:50; Santa Cruz, Cat# sc14394), pig anti-vGlut1 (1:1000, Millipore, Cat# AB5905), and mouse anti-GAD 67 (1:500,

Millipore, Cat# MAB5406). For ISH experiments, sections were hybridized to the target RNA probes complementary to GFP (Multiplex Reagent Kit, Cat# 400281), vGlut1 (Multiplex Reagent Kit, Cat# 317001) or OxR2 (Multiplex Reagent Kit, Cat# 460881). See *SI Appendix* for details.

Quantitative Real-Time RT-PCR. RNA was isolated from either N2A cells or ACC tissue using TRIzol (Invitrogen), and real-time PCR was carried out according to the manufacturer's instructions. Primers for all the target genes are listed in the *SI Appendix*, Supplementary Materials and Methods. See *SI Appendix* for details.

Generation and Validation of AAV2 Cre-Dependent OxR2 Viral Constructs. A miR-based approach was employed to create an effective Cre-dependent knockdown virus for OxR2. We used a nonconditional DNA construct for OxR2 overexpression. See *SI Appendix*, Supplementary Methods for details.

RNA-seq and Bioinformatics Analysis. Total RNA was isolated from ACC samples obtained from SFR and MS female mice using the RNAeasy Mini kit (Qiagen). The differentially expressed genes, GO annotation, functional annotations for biological processes, and PPI network were evaluated. See *SI Appendix* for details.

ELISA. Thirty minutes after the behavioral test, brain tissue samples were collected from the ACC. The Orexin-A kit (FEK-003-30, Phoenix Pharmaceuticals) was used for the ELISA testing. The orexin value of each sample was calculated as pg/mg wet tissue. See *SI Appendix*, Supplementary Methods for details.

In Vitro Whole-Cell Recordings on Brain Slices. Briefly, coronal brain slices of mice containing the ACC or LH (350 μm in thickness) were prepared with a vibratome (Pelco 102, tedpella). Recordings of AP were performed in the current-clamp mode, and the voltage-clamp mode was used to record sEPSCs and PPR via an AxoPatch 200B amplifier (Molecular Devices). See *SI Appendix*, Supplementary Methods for details.

Statistical Analyses. Statistical analyses were conducted using Prism v.6.0 (GraphPad). The normality on each dataset was assessed by the Shapiro–Wilk test, and Levene's test was used to assess the homogeneity of variance. Data that passed these two tests were analyzed using a two-tailed paired or unpaired *t*-test, repeated-measures ANOVA with the post hoc Student–Newman–Keuls test and one-factor ANOVA with Tukey's multiple comparisons test. Nonnormal distribution datasets are analyzed using the nonparametric test (*SI Appendix*, Table S2). Data are shown as the mean with error bars representing the SEM. Differences were considered statistically significant when $P < 0.05$.

Data, Materials, and Software Availability. The RNA-seq datasets analyzed during the current study have been deposited in Figshare repository (https://doi.org/10.6084/m9.figshare.22661803) (49). All other study data are included in the article and/or *SI Appendix*.

ACKNOWLEDGMENTS. The work was funded by National Natural Science Foundation of China (32260202).

1. S. J. Lupien, B. S. McEwen, M. R. Gunnar, C. Heim, Effects of stress throughout the lifespan on the brain, behaviour and cognition. *Nat. Rev. Neurosci.* **10**, 434–445 (2009).
2. M. Popoli, Z. Yan, B. S. McEwen, G. Sanacora, The stressed synapse: The impact of stress and glucocorticoids on glutamate transmission. *Nat. Rev. Neurosci.* **13**, 22–37 (2011).
3. P. Pechtel, D. A. Pizzagalli, Effects of early life stress on cognitive and affective function: An integrated review of human literature. *Psychopharmacology (Berl)* **214**, 55–70 (2011).
4. M. H. Teicher, J. A. Samson, C. M. Anderson, K. Ohashi, The effects of childhood maltreatment on brain structure, function and connectivity. *Nat. Rev. Neurosci.* **17**, 652–666 (2016).
5. C. Heim, C. B. Nemeroff, Neurobiology of early life stress: Clinical studies. *Semin. Clin. Neuropsychiatry* **7**, 147–159 (2002).
6. A. M. Dettmer *et al.*, Associations between early life experience, chronic HPA axis activity, and adult social rank in rhesus monkeys. *Soc. Neurosci.* **12**, 92–101 (2017).
7. S. van Heukelum *et al.*, Where is cingulate cortex? A cross-species view. *Trends Neurosci.* **43**, 285–299 (2020).
8. G. Dolen, A. Darvishzadeh, K. W. Huang, R. C. Malenka, Social reward requires coordinated activity of nucleus accumbens oxytocin and serotonin. *Nature* **501**, 179–184 (2013).
9. L. A. Gunaydin *et al.*, Natural neural projection dynamics underlying social behavior. *Cell* **157**, 1535–1551 (2014).
10. B. A. Vogt, E. A. Nimchinsky, L. J. Vogt, P. R. Hof, Human cingulate cortex: Surface features, flat maps, and cytoarchitecture. *J. Comp. Neurol.* **359**, 490–506 (1995).
11. M. A. Apps, M. F. Rushworth, S. W. Chang, The anterior cingulate gyrus and social cognition: Tracking the motivation of others. *Neuron* **90**, 692–707 (2016).
12. B. Guo *et al.*, Anterior cingulate cortex dysfunction underlies social deficits in Shank3 mutant mice. *Nat. Neurosci.* **22**, 1223–1234 (2019).
13. S. W. Chang, J. F. Gariepy, M. L. Platt, Neuronal reference frames for social decisions in primate frontal cortex. *Nat. Neurosci.* **16**, 243–250 (2013).
14. N. I. Eisenberger, M. D. Lieberman, K. D. Williams, Does rejection hurt? An FMRI study of social exclusion. *Science* **302**, 290–292 (2003).
15. D. W. Hedges, F. L. Woon, Early-life stress and cognitive outcome. *Psychopharmacology (Berl)* **214**, 121–130 (2011).
16. B. P. Ramos, L. A. Colgan, E. Nou, A. F. Arnsten, Beta2 adrenergic agonist, clenbuterol, enhances working memory performance in aging animals. *Neurobiol. Aging* **29**, 1060–1069 (2008).
17. D. Kim *et al.*, Distinct roles of parvalbumin- and somatostatin-expressing interneurons in working memory. *Neuron* **92**, 902–915 (2016).
18. M. G. Zhao *et al.*, Roles of NMDA NR2B subtype receptor in prefrontal long-term potentiation and contextual fear memory. *Neuron* **47**, 859–872 (2005).
19. T. Tan *et al.*, Neural circuits and activity dynamics underlying sex-specific effects of chronic social isolation stress. *Cell Rep.* **34**, 108874 (2021).
20. T. L. Kash *et al.*, Neuropeptide regulation of signaling and behavior in the BNST. *Mol. Cells* **38**, 1–13 (2015).
21. A. J. Grippo *et al.*, Social isolation induces behavioral and neuroendocrine disturbances relevant to depression in female and male prairie voles. *Psychoneuroendocrinology* **32**, 966–980 (2007).
22. L. de Lecea *et al.*, The hypocretins: Hypothalamus-specific peptides with neuroexcitatory activity. *Proc. Natl. Acad. Sci. U.S.A.* **95**, 322–327 (1998).
23. J. P. Kukkonen, C. S. Leonard, Orexin/hypocretin receptor signalling cascades. *Br J. Pharmacol.* **171**, 314–331 (2014).
24. S. B. Li, J. R. Jones, L. de Lecea, Hypocretins, neural systems, physiology, and psychiatric disorders. *Curr. Psychiatry Rep.* **18**, 7 (2016).
25. C. Peyron *et al.*, Neurons containing hypocretin (orexin) project to multiple neuronal systems. *J. Neurosci.* **18**, 9996–10015 (1998).
26. H. Xu *et al.*, A disinhibitory microcircuit mediates conditioned social fear in the prefrontal cortex. *Neuron* **102**, 668–682.e665 (2019).
27. A. Etkin, K. E. Prater, F. Hoeft, V. Menon, A. F. Schatzberg, Failure of anterior cingulate activation and connectivity with the amygdala during implicit regulation of emotional processing in generalized anxiety disorder. *Am. J. Psychiatry* **167**, 545–554 (2010).
28. S. W. White, D. Oswald, T. Ollendick, L. Scahill, Anxiety in children and adolescents with autism spectrum disorders. *Clin. Psychol. Rev.* **29**, 216–229 (2009).
29. S. J. Kang *et al.*, Bidirectional modulation of hyperalgesia via the specific control of excitatory and inhibitory neuronal activity in the ACC. *Mol. Brain* **8**, 81 (2015).
30. B. Toor, L. B. Ray, A. Pozzobon, S. M. Fogel, Sleep, orexin and cognition. *Front. Neurol. Neurosci.* **45**, 38–51 (2021).
31. Z. J. Wang *et al.*, Molecular and cellular mechanisms for differential effects of chronic social isolation stress in males and females. *Mol. Psychiatry* **27**, 3056–3068 (2022).
32. M. E. Flanigan *et al.*, Orexin signaling in GABAergic lateral habenula neurons modulates aggressive behavior in male mice. *Nat. Neurosci.* **23**, 638–650 (2020).
33. H. Feng *et al.*, Orexin signaling modulates synchronized excitation in the sublaterodorsal tegmental nucleus to stabilize REM sleep. *Nat. Commun.* **11**, 3661 (2020).
34. L. Brundin, M. Bjorkqvist, A. Petersen, L. Traskman-Bendz, Reduced orexin levels in the cerebrospinal fluid of suicidal patients with major depressive disorder. *Eur. Neuropsychopharmacol* **17**, 573–579 (2007).
35. L. A. Grafe, A. Cornfeld, S. Luz, R. Valentino, S. Bhatnagar, Orexins mediate sex differences in the stress response and in cognitive flexibility. *Biol. Psychiatry* **81**, 683–692 (2017).
36. O. Johren, S. J. Neidert, M. Kummer, P. Dominiak, Sexually dimorphic expression of prepro-orexin mRNA in the rat hypothalamus. *Peptides* **23**, 1177–1180 (2002).
37. G. C. Harris, M. Wimmer, G. Aston-Jones, A role for lateral hypothalamic orexin neurons in reward seeking. *Nature* **437**, 556–559 (2005).
38. T. C. Chou *et al.*, Orexin (hypocretin) neurons contain dynorphin. *J. Neurosci.* **21**, RC168 (2001).
39. G. B. Kaplan, G. A. Lakis, H. Zhoba, Sleep-wake and arousal dysfunctions in post-traumatic stress disorder: Role of orexin systems. *Brain Res. Bull.* **186**, 106–122 (2022).
40. T. W. Elston, D. K. Bilkey, Anterior cingulate cortex modulation of the ventral tegmental area in an effort task. *Cell Rep.* **19**, 2220–2230 (2017).
41. D. Chaudhury *et al.*, Rapid regulation of depression-related behaviours by control of midbrain dopamine neurons. *Nature* **493**, 532–536 (2013).
42. D. D. Shi *et al.*, Predictable maternal separation confers adult stress resilience via the medial prefrontal cortex oxytocin signaling pathway in rats. *Mol. Psychiatry* **26**, 7296–7307 (2021).
43. C. Toddes, E. M. Lefevre, D. D. Brandner, L. Zugschwert, P. E. Rothwell, mu-opioid receptor (oprm1) copy number influences nucleus accumbens microcircuitry and reciprocal social behaviors. *J. Neurosci.* **41**, 7965–7977 (2021).
44. M. Benekareddy *et al.*, Identification of a corticohabenular circuit regulating socially directed behavior. *Biol. Psychiatry* **83**, 607–617 (2018).
45. R. M. Chemelli *et al.*, Narcolepsy in orexin knockout mice: Molecular genetics of sleep regulation. *Cell* **98**, 437–451 (1999).
46. W. J. Herring *et al.*, Suvorexant in patients with insomnia: Results from two 3-month randomized controlled clinical trials. *Biol. Psychiatry* **79**, 136–148 (2016).
47. P. Malherbe *et al.*, Biochemical and behavioural characterization of EMPA, a novel high-affinity, selective antagonist for the OX(2) receptor. *Br J. Pharmacol.* **156**, 1326–1341 (2009).
48. M. I. Beig, B. W. Dampney, P. Carrive, Both Ox1r and Ox2r orexin receptors contribute to the cardiovascular and locomotor components of the novelty stress response in the rat. *Neuropharmacology* **89**, 146–156 (2015).
49. F. Luo, GSM5857673.zip. Figshare. https://doi.org/10.6084/m9.figshare.22661803. Deposited 20 April 2023.